Dynamic stability of complex networks

Supplementary information

August 12, 2020

Contents

1 The Jacobian ensemble $\mathbb{E}(A_{ij}, \Omega)$ **1**

1.1 The fixed-points $\mathbf{x}^*$ . . . 1

1.1.1 Evaluating $\langle M_2(x) \rangle_\odot$ . . . 4

1.2 Diagonal terms D_{ii} . . . 6

1.3 The off-diagonal terms W_{ij} . . . 8

1.4 Piecing together the J_{ij} puzzle . . . 9

1.4.1 Impact of $P(k)$ and κ_{nn} . . . 11

2 Analyzing the dynamic models **13**

2.1 Social dynamics . . . 13

2.2 Regulatory dynamics . . . 14

2.3 Ecological dynamics . . . 16

2.4 Biochemical dynamics . . . 18

3 Principle eigenvalue of $J_{ij} \in \mathbb{E}(A_{ij}, \Omega)$ **20**

3.1 The role of topology vs. dynamics . . . 26

3.2 Stability classifier S under negative interactions . . . 27

4 Methods and data analysis **28**

4.1 Numerical integration . . . 28

4.2 Numerically estimating J_{ij} . . . 28

4.3 Logarithmic binning . . . 29

4.4 Model and empirical networks . . . 30

5 Mixed dynamics **31**

1 The Jacobian ensemble $\mathbb{E}(A_{ij}, \Omega)$

To analyze complex system stability we seek the *real* Jacobian matrix J_{ij}, as extracted from the system's specific nonlinear interaction mechanisms. We first rewrite Eq. (6) of the main text as

$$\frac{\mathrm{d}x_i}{\mathrm{d}t} = F_i\big(\mathbf{x}(t)\big), \tag{1.1}$$

where

$$F_i\big(\mathbf{x}(t)\big) = M_0\big(x_i(t)\big) + \sum_{j=1}^{N} A_{ij} M_1\big(x_i(t)\big) M_2\big(x_j(t)\big). \tag{1.2}$$

We denote (1.1)'s fixed-point(s) by $\mathbf{x}^* = (x_1, \dots x_N)^\top$, where we omit the the term t to capture their independence on time. These fixed-points are obtained by solving the equilibrium equation

$$F_i(\mathbf{x}^*) = 0. \tag{1.3}$$

To assess the dynamic stability of each of (1.3)'s solutions we track their response to small perturbations, via the Jacobian

$$J_{ij} = \left.\frac{\partial F_i(\mathbf{x})}{\partial x_j}\right|_{\mathbf{x}=\mathbf{x}^*}, \tag{1.4}$$

whose structure we obtain below. Writing

$$J = A \otimes W - I \otimes D \tag{1.5}$$

we treat separately the diagonal terms $J_{ii} = D_{ii}$ and the off-diagonal terms $J_{ij} = A_{ij} W_{ij}$ (I is the identity matrix and $\otimes$ is the Hadamard product).

1.1 The fixed-points $\mathbf{x}^*$

We consider systems of the form (1.1) that exhibit at least one fully positive fixed-point $\mathbf{x}^*$. Using Eq. (1.3) we write

$$M_0(x_i) + \sum_{j=1}^{N} A_{ij} M_1(x_i) M_2(x_j) = 0, \tag{1.6}$$

which can be expressed as

$$R(x_i)\sum_{j=1}^{N} A_{ij}M_2(x_j) = 1, \tag{1.7}$$

where

$$R(x_i) = -\frac{M_1(x_i)}{M_0(x_i)}. \tag{1.8}$$

Denoting i's degree by $k_i = \sum_{j=1}^{N} A_{ij}$ we write (1.7) as

$$R(x_i) = \frac{1}{k_i\langle M_2(x)\rangle_{i,\odot}}, \tag{1.9}$$

in which

$$\langle M_2(x)\rangle_{i,\odot} = \frac{1}{k_i}\sum_{j=1}^{N} A_{ij}M_2(x_j) \tag{1.10}$$

represents an average of the function $M_2(x_j)$ over all of node i's direct network *neighborhood*, which we captured by the $\odot$ symbol. Assuming the function $R(x)$ is invertible around x_i we obtain i's fixed-point activity as

$$x_i = R^{-1}(q_i), \tag{1.11}$$

where $R^{-1}(x)$ is the inverse function of $R(x)$ and

$$q_i = \frac{1}{k_i\langle M_2(x)\rangle_{i,\odot}} \tag{1.12}$$

is i's inverse degree, which approaches zero in the limit of large k_i.

To understand the dependence of activity on degree, we seek the average steady-state activity over all nodes with degree k as

$$x(k) = \frac{1}{|\mathbf{G}(k)|}\sum_{i\in\mathbf{G}(k)} x_i, \tag{1.13}$$

where $\mathbf{G}(k) = \{i \in [1, N] | k_i = k\}$ is the group of all nodes with degree k, and $|\mathbf{G}(k)|$ is the number of nodes in that group. To approximate $x(k)$ we first evaluate the average neighborhood activity of all nodes in $\mathbf{G}(k)$ via

$$\langle M_2(x)\rangle_{k,\odot} = \frac{1}{|\mathbf{G}(k)|}\sum_{i\in\mathbf{G}(k)} \langle M_2(x)\rangle_{i,\odot}, \tag{1.14}$$

capturing the average value of $M_2(x)$ surrounding nodes with degree k. Most generally, the activities x_j may depend, to some extent, on the degree k_i of their neighbor i, however this dependence is often unknown, and, most importantly, relatively weak [1]. Indeed, i is but one of j's k_j neighbors, who are typically a random selection, representative of the network's degree distribution [2]. Therefore, i's degree k_i is only weakly correlated with j's activity x_j. To capture this dependence we approximate (1.14) as

$$\langle M_2(x)\rangle_{k,\odot} \approx f(k)\langle M_2(x)\rangle_{\odot}, \tag{1.15}$$

where

$$\langle M_2(x)\rangle_{\odot} = \frac{1}{N}\sum_{i=1}^{N}\frac{1}{k_i}\sum_{j=1}^{N} A_{ij}M_2(x_j) \tag{1.16}$$

represents the average of the function $M_2(x_j)$ over *all* network neighborhoods, independent of i or k. In (1.15) the term $\langle M_2(x)\rangle_{\odot}$ captures a characteristic aggregated function of the system's fixed-point, capturing the value of $M_2(x_j)$ averaged over all nearest neighbor nodes, but not specifically over i's neighbors - hence the approximation sign $\approx$, rather than $=$. The function $f(k)$ corrects this average to account for the fact that in in the l.h.s. of (1.15) the average is carried out selectively over nodes whose neighbor has degree k. For example, $f(k) = 1$ represents the *perfect* case of no degree-correlations, under which x_j is fully independent of its neighbor's degree k. More generally, we assume $f(k)$ to be a *weak* function, *i.e.* sub-polynomial in k, for example

$$f(k) \sim \log^n(k). \tag{1.17}$$

We can now approximate $x(k)$ in (1.13), taking x_i from (1.11), and $\langle M_2(x)\rangle_{i,\odot}$ from (1.15) to obtain

$$x(k) = R^{-1}(q), \tag{1.18}$$

where

$$q = \frac{1}{f(k)\langle M_2(x)\rangle_{\odot}k}. \tag{1.19}$$

In the asymptotic limit of large k, the sub-polynomial contribution of $f(k)$ becomes negligible, and hence we have

$$q \sim \langle M_2(x)\rangle_{\odot}^{-1}k^{-1}. \tag{1.20}$$

1.1.1 Evaluating $\langle M_2(x)\rangle_\odot$

To link $\langle M_2(x)\rangle_\odot$ to the network A_{ij} we use a mean-field approximation. We first define the nearest neighbor activity as

$$x_{\rm nn} = \langle x\rangle_\odot = \frac{1}{N}\sum_{i=1}^{N}\frac{1}{k_i}\sum_{j=1}^{N}A_{ij}x_j, \tag{1.21}$$

and its corresponding nearest neighbor degree as

$$\kappa_{\rm nn} = \langle k\rangle_\odot = \frac{1}{N}\sum_{i=1}^{N}\frac{1}{k_i}\sum_{j=1}^{N}A_{ij}k_j. \tag{1.22}$$

Hence, the average nearest neighbor node is characterized by activity $x_{\rm nn}$ and degree $\kappa_{\rm nn}$. While $x_{\rm nn}$ depends on the system's dynamics (1.1), $\kappa_{\rm nn}$ is fully determined by the topology A_{ij}, linked to the network's degree distribution $P(k)$. In the absence of degree correlations we have [3]

$$\kappa_{\rm nn} = \frac{\langle k^2\rangle}{\langle k\rangle}, \tag{1.23}$$

with $\langle k^n\rangle$ capturing the nth moment of $P(k)$. For a homogeneous network in which $P(k)$ is bounded we have $\kappa_{\rm nn}\approx\langle k\rangle$, however, if the network is highly heterogeneous, *i.e.* $P(k)$ is fat-tailed - as indeed, many real networks are [4] - we find that $\kappa_{\rm nn}\gg\langle k\rangle$. More generally, in case the network has degree correlations we write [5]

$$\kappa_{\rm nn} = \sum_{k'=1}^{\infty}\sum_{k=1}^{\infty}kP(k|k')P(k') \tag{1.24}$$

in which the conditional probability $P(k|k')$ captures the dependence between neighboring nodes. In both cases, (1.23) and the more general (1.24), under extreme degree-heterogeneity, κ may diverge with system size as [2]

$$\kappa_{\rm nn}\sim N^{\beta}. \tag{1.25}$$

We can now link $\langle M_2(x)\rangle_\odot$ in (1.16) to $\kappa_{\rm nn}$ and $x_{\rm nn}$, as, indeed, $\langle M_2(x)\rangle_\odot$ is designed to capture the mean value of $M_2(x)$ over all nearest neighbor nodes, namely nodes with typical degree $\kappa_{\rm nn}$ and activity $x_{\rm nn}$. We, therefore, approximate (1.16) as

$$\langle M_2(x)\rangle_\odot \approx M_2(x_{\rm nn}), \tag{1.26}$$

in which we swap the order of operations from $\langle M_2(x)\rangle$ to $M_2(\langle x\rangle)$. Such approximation becomes exact in the limit where $M_2(x)$ is linear or when x_j are narrowly distributed. For

example, in our Biochemical model we have $M_2(x_j) = x_j$, a linear function, and in our Social model the activities x_j are bounded, hence narrowly distributed between zero and unity. Approximation (1.26) is also justified when $M_2(x)$ is sub-linear, *e.g.*, a saturating function $M_2(x \to \infty) \to 1$. Such saturation is present, for instance, in our Regulatory and Ecological dynamics. Under these conditions, even if x_j are broadly distributed, $M_2(x_j)$ are uniform, and hence their average is (roughly) concentrated around $M_2(\langle x \rangle)$. For a super-linear $M_2(x)$, combined with broadly distributed x_j, approximation (1.26) becomes inaccurate.

To evaluate $M_2(x_{\rm nn})$'s dependence on $\kappa_{\rm nn}$ we use (1.9) to write

$$R(x_{\rm nn}) = \frac{1}{\kappa_{\rm nn} f(\kappa_{\rm nn}) M_2(x_{\rm nn})}, \tag{1.27}$$

where we substitute $\langle M_2(x) \rangle_{i,\odot}$ by $f(\kappa_{\rm nn}) M_2(x_{\rm nn})$ following approximations (1.15) and (1.26), and use the nearest neighbor degree $\kappa_{\rm nn}$ in place of k. We therefore arrive at

$$Z(x_{\rm nn}) = \frac{1}{f(\kappa_{\rm nn})\kappa_{\rm nn}} \equiv q_\odot, \tag{1.28}$$

where $Z(x) = R(x)M_2(x)$ is a dynamic function, fully determined by $M_0(x), M_1(x)$ and $M_2(x)$ in (1.1). In (1.29) we use the notation $q_\odot$ to signify the inverse degree (q) associated with the typical *neighborhood* ($\odot$). By inversion we obtain

$$x_{\rm nn} = Z^{-1}(q_\odot), \tag{1.29}$$

and hence

$$M_2(x_{\rm nn}) = M_2\big(Z^{-1}(q_\odot)\big). \tag{1.30}$$

To obtain the asymptotic scaling of $M_2(x_{\rm nn})$ on $\kappa_{\rm nn}$ we use the Hahn expansion [6] to express $Z(x)$ in the form of a power series around $q_\odot \to 0$, *i.e.* $\kappa_{\rm nn} \to \infty$. Hence we write

$$M_2\big(Z^{-1}(q_\odot)\big) = \sum_{n=0}^{\infty} G_n q_\odot^{\Psi(n)}, \tag{1.31}$$

where $\Psi(n)$ is a set of real powers in ascending order with n. In the limit of large $\kappa_{\rm nn}$ (small $q_\odot$) the expansion in (1.31) is dominated by the leading power $\Psi(0)$, predicting that

$$M_2(x_{\rm nn}) \sim \kappa_{\rm nn}^{\xi}, \tag{1.32}$$

where

$$\xi = -\Psi(0). \tag{1.33}$$

The exponent ξ is fully determined by the dynamic functions $M_0(x), M_1(x)$ and $M_2(x)$ through the Hahn expansion in (1.31). It is independent of A_{ij}, as well as of other microscopic parameters, such as the specific rate-constants used in (1.1), which are encapsulated within the *coefficients* G_n, but have no impact on the *powers* $\Psi(n)$.

Using approximation (1.26) we substitute $M_2(x_{\rm nn})$ in (1.32), to replace the $\langle M_2(x)\rangle_\odot$ term in the denominator of Eq. (1.19), obtaining

$$q \sim \kappa_{\rm nn}^{-\xi} k^{-1}. \tag{1.34}$$

Next we use these results, specifically (1.18) and (1.34), to obtain the terms of the Jacobian, J_{ij} and J_{ii}, and their dependence on $\kappa_{\rm nn}$ and k.

1.2 Diagonal terms D_{ii}

Using (1.2) and (1.4) we write the diagonal Jacobian terms as

$$D_{ii} = \left.\frac{\partial F_i(\mathbf{x})}{\partial x_i}\right|_{\mathbf{x}=\mathbf{x}^*} = \left.\left(M_0'(x_i) + M_1'(x_i)\sum_{j=1}^{N} A_{ij} M_2(x_j)\right)\right|_{\mathbf{x}=\mathbf{x}^*}, \tag{1.35}$$

where $M_0'(x) = \partial M_0/\partial x$ and $M_1'(x) = \partial M_1/\partial x$. Next we use (1.10) to express the sum on the r.h.s. obtaining

$$D_{ii} = \left. M_0'(x_i)\right|_{\mathbf{x}=\mathbf{x}^*} + \left. M_1'(x_i) k_i \langle M_2(x)\rangle_{i,\odot}\right|_{\mathbf{x}=\mathbf{x}^*}, \tag{1.36}$$

in which we substitute the summation by the neighbor average $\langle M_2(x)\rangle_{i,\odot}$. Finally, expressing the fixed-point $\mathbf{x}^*$ via (1.11) and averaging over all nodes with degree k as done in (1.13) - (1.19), we arrive at

$$D(k) = M_0'\big(R^{-1}(q)\big) + k M_1'\big(R^{-1}(q)\big) f(k) \langle M_2(x)\rangle_\odot, \tag{1.37}$$

capturing the average diagonal term D_{ii}, associated with a node $i \in \mathbf{G}(k)$.

Next we use (1.8) to write $M_0(x) = -M_1(x)/R(x)$, which provides

$$M_0'(x) = -\frac{M_1'(x)}{R(x)} + \frac{M_1(x)R'(x)}{R^2(x)}. \tag{1.38}$$

Substituting (1.38) and (1.19) into (1.37) we arrive at

$$D(k) = -\frac{M_1'\big(R^{-1}(q)\big)}{q} + \frac{M_1\big(R^{-1}(q)\big)R'\big(R^{-1}(q)\big)}{q^2} + \frac{M_1'\big(R^{-1}(q)\big)}{q}, \tag{1.39}$$

where we used the fact that $R(R^{-1}(q)) = q$. Collecting all terms we write

$$D(k) = \frac{1}{q^2} Y\big(R^{-1}(q)\big), \tag{1.40}$$

where $Y(x) = M_1(x)R'(x)$, similar to $Z(x)$ above, is a dynamic function fully determined by $M_0(x)$ and $M_1(x)$, independent of A_{ij}.

To obtain the asymptotic scaling of $D(k)$ with k we, once again, use the Hahn expansion to express $Y(x)$ in the form of a power series around $q \to 0$, *i.e.* $k \to \infty$. Writing

$$Y\big(R^{-1}(q)\big) = \sum_{n=0}^{\infty} C_n q^{\Gamma(n)}, \tag{1.41}$$

we obtain the leading power in the expansion of $D(k)$ as $D(k) \sim q^{-2+\Gamma(0)}$, exact up to higher powers in q, which vanish under $q \to 0$. Using the scaling of Eq. (1.34), this predicts

$$D(k) \sim \kappa_{\mathrm{nn}}^{\xi\mu} k^{\mu}, \tag{1.42}$$

where

$$\mu = 2 - \Gamma(0), \tag{1.43}$$

and ξ is taken from (1.33).

Equation (1.42), valid in the limit of large κ_{nn} and k, captures the typical magnitude of the diagonal terms D_{ii}, and their dependence on each node i's degree k_i. The scaling exponents μ and ξ are fully determined by $\Gamma(n)$ in (1.41) and $\Psi(n)$ in (1.31), namely they are affected by the *powers* of the dynamic functions $M_0(x)$ and $M_1(x)$. At the same time μ and ξ are independent of the *coefficients* C_n, G_n, hence they are not sensitive to specific parameters, such as rate constants in (1.1). While Eq. (1.42) provides the *scaling* with k, $D(k)$'s specific magnitude may, generally, depend on the coefficients, however for sufficiently large k, such dependencies have little impact on the spectrum of J_{ij}. Finally, the sign of $D(k)$, positive or negative, is determined by $Y(x)$, which, in turn depends on $M_0(x)$ and $M_1(x)$. Stability can only be ensured in case $D(k) < 0$, *i.e.* negative self-feedback, and hence below we write

$$D(k) \sim -C\kappa_{\mathrm{nn}}^{\xi\mu} k^{\mu}, \tag{1.44}$$

where $C > 0$ (see more detailed discussion in Sec. 1.4).

1.3 The off-diagonal terms W_{ij}

The off-diagonal Jacobian terms are given by

$$W_{ij} = \frac{\partial F_i(\mathbf{x})}{\partial x_j}\bigg|_{\mathbf{x}=\mathbf{x}^*} = \frac{\partial}{\partial x_j}\left(M_0(x_i) + M_1(x_i)\sum_{j=1}^{N} A_{ij}M_2(x_j)\right)\bigg|_{\mathbf{x}=\mathbf{x}^*}. \tag{1.45}$$

Collecting only the terms that explicitly depend on x_j we obtain

$$W_{ij} = M_1(x_i)A_{ij}M_2'(x_j)\Big|_{\mathbf{x}=\mathbf{x}^*}, \tag{1.46}$$

which, taking the fixed-point activities from (1.11) provides

$$W_{ij} = M_1\big(R^{-1}(q_i)\big)A_{ij}M_2'\big(R^{-1}(q_j)\big). \tag{1.47}$$

We seek the average dependence of W_{ij} on the degrees k_i and k_j, hence we consider the group $\mathbf{G}(k_1,k_2) = \{(i,j)|k_i = k_1; k_j = 2; A_{ij} = 1\}$, comprising all links ($A_{ij} = 1$) linking nodes with degrees k_1, k_2. We then average over the relevant Jacobian term as

$$W(k_1,k_2) = \frac{1}{|\mathbf{G}(k_1,k_2)|}\sum_{(i,j)\in\mathbf{G}(k_1,k_2)} W_{ij}, \tag{1.48}$$

allowing us to evaluate the magnitude of an average (non zero) term whose row index is associated with a node of degree k_1, and whose column index is associated with a node of degree k_2. Using (1.46) we write

$$W(k_1,k_2) = \frac{1}{|\mathbf{G}(k_1,k_2)|}\sum_{(i,j)\in\mathbf{G}(k_1,k_2)} M_1(x_i)A_{ij}M_2'(x_j) = \langle M_1(x_i)M_2'(x_j)\rangle_{\mathbf{G}(k_1,k_2)}, \tag{1.49}$$

a product average over all node pairs in $\mathbf{G}(k_1,k_2)$. In case the two activities x_i and x_j are uncorrelated, we can approximate the r.h.s. of (1.49) by a product over the single averages, *i.e.* $\langle M_1(x_i)\rangle_{\mathbf{G}(k_1,k_2)}\langle M_2'(x_j)\rangle_{\mathbf{G}(k_1,k_2)}$. Each of these averages can be then evaluated by

$$\langle M_1(x_i)\rangle_{\mathbf{G}(k_1,k_2)} \approx M_1\big(R^{-1}(q_1)\big) \tag{1.50}$$

$$\langle M_2'(x_j)\rangle_{\mathbf{G}(k_1,k_2)} \approx M_2'\big(R^{-1}(q_2)\big), \tag{1.51}$$

where we use the fact that in $\mathbf{G}(k_1,k_2)$ the activity x_i is on average $R^{-1}(q_1)$, i.e. $x(k_1)$ (1.13), and the activity x_j is $R^{-1}(q_2)$, namely $x(k_2)$. In reality, however, the two activities are, to some extent, correlated by virtue of being nearest neighbors ($A_{ij} = 1$). We therefore follow a similar track as in (1.15) and write (1.49) as

$$W(k_1, k_2) \approx f(k_1, k_2) M_1\big(R^{-1}(q_1)\big) M_2'\big(R^{-1}(q_2)\big), \tag{1.52}$$

capturing the k_1, k_2 correlations via the sub-polynomial function $f(k_1, k_2)$.

We can now obtain the scaling of $W(k_1, k_2)$ by examining the behavior of $M_1\big(R^{-1}(q_1)\big)$ and $M_2'\big(R^{-1}(q_2)\big)$ in the limit of large k_1 and k_2, or subsequently small q_1, q_2. We, therefore express these functions via the Hahn expansion as

$$M_1\big(R^{-1}(q)\big) = \sum_{n=0}^{\infty} K_n q^{\Pi(n)} \tag{1.53}$$

$$M_2'\big(R^{-1}(q)\big) = \sum_{n=0}^{\infty} L_n q^{\Theta(n)}, \tag{1.54}$$

and take only the leading term in the limit $q \to 0$, providing

$$W(k_1, k_2) = f(k_1, k_2) K_0 q_1^{\Pi(0)} L_0 q_2^{\Theta(0)} + \cdots . \tag{1.55}$$

As we are only interested in the asymptotic scaling with k_1, k_2 we neglect all terms that do not contribute the scaling, namely $f(k_1, k_2), K_0$ and L_0. Finally, substituting q with $\kappa_{\mathrm{nn}}^{-\xi} k^{-1}$ as per Eq. (1.34), we obtain

$$W(k_1, k_2) \sim \kappa_{\mathrm{nn}}^{\xi(\nu+\rho)} k_1^{\nu} k_2^{\rho} \tag{1.56}$$

where

$$\nu = -\Pi(0), \quad \rho = -\Theta(0), \tag{1.57}$$

and ξ is taken from (1.33).

1.4 Piecing together the J_{ij} puzzle

We have now obtained the interplay between structure and dynamics, expressed through the magnitude of the diagonal/off-diagonal Jacobian entries, and their dependence on the network's degree distribution via k_i, k_j and κ_{nn}. This dependence is given in terms of asymptotic scaling relationships, as captured by the model dependent exponents μ, ν, ρ, ξ. This leaves a degree of freedom, determined by the specific parameters of each model to add an arbitrary coefficient as a pre-factor to the actual J_{ij} terms. For example, the expression $D(k) \sim -C\kappa_{\mathrm{nn}}^{\xi\mu} k^{\mu}$ in Eq. (1.42) should be taken to mean

$$D(k) = -C(\kappa_{\mathrm{nn}}, k) \kappa_{\mathrm{nn}}^{\xi\mu} k^{\mu} + \cdots \tag{1.58}$$

where $C(\kappa_{\rm nn}, k)$ is a sub-polynomial function, which is roughly constant, *i.e.* $C(\kappa_{\rm nn}, k) \approx C$, and $\cdots$ represents *lower* powers of $\kappa_{\rm nn}$ and k, that are negligible in the asymptotic limit. In the context of stability the diagonal terms of J_{ij} are assumed to be negative, capturing a stabilizing negative feedback, hence the $-C$ term in (1.58), which is negative if $C > 0$.

We can now piece our results together to construct the complete Jacobian as appears in Eq. (1.5), rewriting it as

$$J_{ij} = A_{ij}W_{ij} + \delta_{ij}D_{ii} = -\delta_{ij}C\kappa_{\rm nn}^{\xi\mu}k_i^{\mu} + A_{ij}\kappa_{\rm nn}^{\xi(\nu+\rho)}k_i^{\nu}k_j^{\rho}, \tag{1.59}$$

where the first term on the r.h.s. represents the (negative) diagonal entries, and second term captures the off-diagonal entries, which are non-zero only if $A_{ij} = 1$; δ_{ij} is the Kronecker delta function. As we are only interested in the sign of the principle eigenvalue, but not in its specific magnitude, we have the degree of freedom to multiply J_{ij} by an arbitrary constant. We therefore normalize J_{ij} by $\kappa_{\rm nn}^{-\xi(\nu+\rho)}$, providing

$$J_{ii} \sim -C\kappa_{\rm nn}^{\eta}k_i^{\mu} \tag{1.60}$$

$$J_{ij} \sim A_{ij}k_i^{\nu}k_j^{\rho} \tag{1.61}$$

for the diagonal and off-diagonal terms respectively, with $\eta = \xi(\mu - \nu - \rho)$ - recovering Eqs. (7) and (8) of the main text.

Equations (1.60) and (1.61) describe the asymptotic structure of the diagonal and off-diagonal Jacobian terms, as extracted from the general dynamics of Eq. (1.1). The resulting J_{ij} is characterized by several distinct structural and dynamic inputs: A_{ij}, the network topology, which determines the non-vanishing off-diagonal elements. It also determines the degrees k_i, k_j and the average neighbor degree $\kappa_{\rm nn}$. The exponents

$$\Omega = (\eta, \mu, \nu, \rho) \tag{1.62}$$

are fully independent of the network topology, extracted from the dynamic functions $M_0(x), M_1(x)$ and $M_2(x)$, *i.e.* the interaction mechanisms driving Eq. (1.1). These exponents are universal in the sense that they do not depend of the specific model *parameters*, but rather on the *model* itself, *e.g.*, Social, Regulatory etc. The coefficient C, in contrast, is non-universal, and its value is determined by the specific rate-constants and time-scales driving Eq. (1.1); here we do not attempt to predict the magnitude of this coefficient. In the limit of sufficiently large k_i and k_j, and, where applicable - in the limit of large $\kappa_{\rm nn}$, the specific finite value of C has negligible impact on the principle eigenvalue of J_{ij} as we explicitly show in Sec. 3. Hence stability is asymptotically determined by the exponents Ω, independent of C. The meaning is that the *model* can be asymptotically stable or unstable, regardless of its specific *parameters*.

1.4.1 Impact of $P(k)$ and $\kappa_{\rm nn}$

In this derivation we considered only the *scaling* of J_{ij} on the degrees k_i, k_j, and on the nearest neighbor degree $\kappa_{\rm nn}$. We disregarded coefficients, such as C_n or G_n in (1.41) and (1.31), or sub-polynomial functions like $f(k)$ in (1.17). The rationale is that in the limit of large degrees the Jacobian spectrum is mainly impacted by these asymptotic scaling relationships, and has little dependence on finite size coefficients that do not scale with $k, \kappa_{\rm nn}$, and hence also do not grow significantly as a function of system size N. Indeed, May's paradox is rooted precisely in such scaling, in which the principle eigenvalue grows asymptotically as $\sim N^c$ (in May's work $c = 1/2$) rendering stability independent of finite coefficients, such as the system's intrinsic time-scales [7]. Therefore, Eqs. (1.60) and (1.61) are especially relevant when $P(k)$ is fat-tailed, *e.g.*, scale-free, where the hub-degrees and the nearest neighbor degree can potentially scale with N.

The role of $\kappa_{\rm nn}$. While k_i is a node specific attribute, that captures a specific dependency between the ith diagonal term and i's degree, the pre-factor $\kappa_{\rm nn}^{\eta}$ represents a network aggregated parameter, indeed - a *constant*, whose impact is often negligible in the asymptotic limit of large k. We include it in our analysis, however, because under extreme degree-heterogeneity, we may observe that $\kappa_{\rm nn}$ diverges as $\kappa_{\rm nn} \sim N^{\beta}$ (1.25), and therefore *can* potentially impact the system stability under $N \to \infty$. For example, in a scale-free network where $P(k) \sim k^{-\gamma}$, we can use $\kappa_{\rm nn} = \langle k^2 \rangle / \langle k \rangle$ in (1.23) to obtain

$$\kappa_{\rm nn} \sim \begin{cases} N & \gamma < 2 \\ N^{3-\gamma} & 2 \leq \gamma < 3 \\ \log(N) & \gamma \geq 3 \end{cases} , \tag{1.63}$$

which scales with N as long as $\gamma < 3$. There are, however, broad conditions, that arise quite naturally in many real systems, in which the $\kappa_{\rm nn}$ term in (1.60) can be neglected, significantly simplifying the stability analysis:

- **Finite** $\kappa_{\rm nn}$. In case $\gamma \geq 3$, $\kappa_{\rm nn}$ no longer scales with N, it behaves as a constant and has no impact in the asymptotic limit. Under these conditions it suffices to write Eq. (1.60) as $J_{ii} \sim -Ck_i^{\mu}$.

- **Bounded activities**. In some models the activities x_i are bounded. For example, in spreading processes, from epidemics to cascading failures, the activities satisfy $0 \leq x_i \leq 1$. Under these conditions the leading power in the power-series expansion of (1.18) is zero, and hence $x(k \to \infty) \sim 1$. The result is that the nearest neighbor activity $x_{\rm nn}$, associated with degree $\kappa_{\rm nn}$ is itself bounded, and even if $\kappa_{\rm nn} \to \infty$ *à la* Eq. (1.63), we still have $x_{\rm nn} \sim 1$. Consequently $M_2(x_{\rm nn})$ in (1.30) also approaches a constant value, and therefore the leading power in the expansion (1.31) is $\Psi(0) = 0$. This provides, based on Eq. (1.33), $\xi = 0$, which in turn leads to $\eta = 0$ in (1.60), again resulting in $J_{ii} \sim -Ck_i^{\mu}$, independent of $\kappa_{\rm nn}$.

- **Saturating** $M_2(x)$. Another common feature in many relevant models is that $M_2(x_j \to \infty) \to 1$. This represents the saturating impact of node j on its nearest neighbor i, as frequently observed in regulatory processes or in population dynamics. Once again, we have $M_2(x_{\rm nn}) \sim 1$, providing $\xi = 0$, and consequently $\eta = 0$ in (1.60).

The ensemble $\mathbb{E}(A_{ij}, \Omega)$ summary

Staring from Eq. (1.1) we use $M_0(x), M_1(x)$ and $M_2(x)$ to construct the functions

$$R(x) = -\frac{M_1(x)}{M_0(x)}, \quad Y(x) = M_1(x)R'(x), \quad Z(x) = R(x)M_2(x). \tag{1.64}$$

From these we extract the four relevant power-series expansions

$$\begin{aligned} M_2\big(Z^{-1}(x)\big) &= \sum_{n=0}^{\infty} G_n x^{\Psi(n)}, \quad Y\big(R^{-1}(x)\big) = \sum_{n=0}^{\infty} C_n x^{\Gamma(n)}, \\ M_1\big(R^{-1}(x)\big) &= \sum_{n=0}^{\infty} K_n x^{\Pi(n)}, \quad M_2'\big(R^{-1}(x)\big) = \sum_{n=0}^{\infty} L_n x^{\Theta(n)} \end{aligned} \tag{1.65}$$

whose leading powers determine the dynamic exponents $\Omega = (\eta, \mu, \nu, \rho)$ as

$$\mu = 2 - \Gamma(0), \quad \nu = -\Pi(0), \quad \rho = -\Theta(0), \quad \eta = -\Psi(0)(\mu - \nu - \rho). \tag{1.66}$$

To construct $J_{ij} \in \mathbb{E}(A_{ij}, \Omega)$ we first generate the network A_{ij}, then extract the degrees k_i of all nodes and the nearest neighbor degree $\kappa_{\rm nn}$ from Eq. (1.22). The resulting J_{ij} satisfies

$$J_{ii} \sim -C\kappa_{\rm nn}^{\eta} k_i^{\mu} \tag{1.67}$$

$$J_{ij} \sim A_{ij} k_i^{\nu} k_j^{\rho}, \tag{1.68}$$

where the constant $C > 0$ is arbitrary.

2 Analyzing the dynamic models

To demonstrate our formalism we examined several commonly used dynamic models, as listed in Fig. 1g of the main text. Below we extract the exponents Ω for each of these models.

2.1 Social dynamics

As an example of Social dynamics we used epidemic spreading via the Susceptible-Infected-Susceptible (SIS) model, in which $x_i(t)$ captures the probability of infection of node i. Denoting the susceptible state by S and the infected state by I, the model includes the following transitions

$$I \xrightarrow{f} S \tag{2.1}$$

$$I + S \xrightarrow{g} 2I, \tag{2.2}$$

capturing the processes of recovery at a rate f and infection at rate g. This gives rise to the dynamic equation [8]

$$\frac{\mathrm{d}x_i}{\mathrm{d}t} = -fx_i + \sum_{j=1}^{N} A_{ij} g(1-x_i)x_j, \tag{2.3}$$

characterized by the dynamic functions $M_0(x) = -fx, M_1(x) = 1-x$ and $M_2(x) = gx$.

To obtain the relevant J_{ij} ensemble, we seek the exponents $\Omega = (\eta, \mu, \nu, \rho)$. We begin by translating the given functions $M_0(x), M_1(x), M_2(x)$ in to the relevant functions shown in (1.64), providing

$$R(x) = -\frac{M_1(x)}{M_0(x)} = \frac{1-x}{fx} \tag{2.4}$$

$$Y(x) = M_1(x)R'(x) = \frac{x-1}{fx^2} \tag{2.5}$$

$$Z(x) = R(x)M_2(x) = \frac{g}{f} - \frac{g}{f}x. \tag{2.6}$$

Inverting $R(x)$ and $Z(x)$, we write

$$R^{-1}(x) = \frac{1}{fx+1}, \tag{2.7}$$

$$Z^{-1}(x) = 1 - \frac{f}{g}x, \tag{2.8}$$

allowing us to construct the Hahn expansions of (1.65) as

$$M_2\big(Z^{-1}(x)\big) = gZ^{-1}(x) = g - fx \tag{2.9}$$

$$Y\big(R^{-1}(x)\big) = \frac{R^{-1}(x) - 1}{f \times \big(R^{-1}(x)\big)^2} = -x - fx^2 \tag{2.10}$$

$$M_1\big(R^{-1}(x)\big) = 1 - R^{-1}(x) = \frac{fx}{fx+1} = fx - f^2x^2 + f^3x^3 - \cdots \tag{2.11}$$

$$M_2'\big(R^{-1}(x)\big) = g. \tag{2.12}$$

Each of these functions is expressed as a Hahn power-series, in some cases a finite polynomial, *e.g.*, (2.9) or (2.10), and in others an infinite series, where we only write the leading terms around $x \to 0$. Here, coincidentally, the last function (2.12) is a constant, with the only power being x^0. We can list the relevant powers in these Hahn expansions as $\Psi(0) = 0, \Gamma(0) = 1, \Pi(0) = 1$ and $\Theta(0) = 0$, which, using (1.66) provides

$$\mu = 2 - \Gamma(0) = 1 \tag{2.13}$$

$$\nu = -\Pi(0) = -1 \tag{2.14}$$

$$\rho = -\Theta(0) = 0 \tag{2.15}$$

$$\eta = -\Psi(0)(\mu - \nu - \rho) = 0. \tag{2.16}$$

2.2 Regulatory dynamics

We used the Michaelis-Menten model to capture gene Regulatory dynamics [9]. Here, Eq. (1.1) tracks the level of gene expression $x_i(t)$, as regulated via the sub-cellular network A_{ij}, providing

$$\frac{\mathrm{d}x_i}{\mathrm{d}t} = -Bx_i^a + \sum_{j=1}^{N} A_{ij}\frac{x_j^h}{1 + x_j^h}. \tag{2.17}$$

The self-dynamic term $M_0(x) = -Bx^a$ captures biochemical processes [10], such as degradation ($a = 1$) or dimerization ($a = 2$). The interaction terms $M_1(x) = 1, M_2(x) = x^h/1 + x^h$ describe genetic activation, a switch-like dynamics, which ranges from $M_2(0) = 0$ to $M_2(x \to \infty) = 1$ to capture activation of gene i by gene j. The Hill coefficient h governs the rate of saturation of $M_2(x)$.

First, we construct the three functions summarized in (1.64):

$$R(x) = -\frac{M_1(x)}{M_0(x)} = \frac{1}{Bx^a} \tag{2.18}$$

$$Y(x) = M_1(x)R'(x) = -\frac{a}{Bx^{a+1}} \tag{2.19}$$

$$Z(x) = R(x)M_2(x) = \frac{x^h}{B(x^a + x^{a+h})}. \tag{2.20}$$

Inverting $R(x)$, we write

$$R^{-1}(x) = B^{-\frac{1}{a}} x^{-\frac{1}{a}}, \tag{2.21}$$

allowing us to construct the Hahn expansions (1.65)

$$Y\big(R^{-1}(x)\big) = -\frac{a}{B}\left(\frac{1}{Bx}\right)^{-\frac{a+1}{a}} = aB^{\frac{1}{a}} x^{\frac{a+1}{a}} \tag{2.22}$$

$$M_1\big(R^{-1}(x)\big) = 1 = x^0 \tag{2.23}$$

$$M_2'\big(R^{-1}(x)\big) = \frac{hB^{-\frac{h-1}{a}} x^{-\frac{h-1}{a}}}{\left(1 + B^{-\frac{h}{a}} x^{-\frac{h}{a}}\right)^2} = hB^{\frac{h+1}{a}} x^{\frac{h+1}{a}} - 2hB^{\frac{2h+1}{a}} x^{\frac{2h+1}{a}} + \cdots . \tag{2.24}$$

In each of these expansions we write the leading terms in the $x \to 0$ limit: in (2.22) and (2.23) the expansion features a single term, *i.e.* a pure monomial, and in (2.24) we show the first two terms of the relevant Hahn expansion. To obtain Ω we extract only the leading *powers* $\Gamma(0) = (a+1)/a, \Pi(0) = 0, \Theta(0) = (h+1)/a$, ignoring the *coefficients*, *e.g.*, $aB^{1/a}$ or $hB^{(h+1)/a}$. We can now use (1.66) to extract the dynamic exponents as

$$\mu = 2 - \Gamma(0) = \frac{a-1}{a} \tag{2.25}$$

$$\nu = -\Pi(0) = 0 \tag{2.26}$$

$$\rho = -\Theta(0) = -\frac{h+1}{a}. \tag{2.27}$$

To obtain η we must calculate $M_2(Z^{-1}(x))$, requiring us to invert the function $Z(x)$ in (2.20), which becomes analytically prohibitive for general a and h. Fortunately, in Regulatory dynamics we can calculate this term directly. We first recall, from Eq. (1.30) that $M_2(Z^{-1}(q_\odot)) = M_2(x_{\rm nn})$, where $x_{\rm nn}$ is the average neighbor activity and $q_\odot \sim 1/\kappa_{\rm nn}$ is the average neighbor degree. For a general node with degree k we can use (1.18) together with (2.21) to write

$$x(k) = B^{-\frac{1}{a}} q^{-\frac{1}{a}} \sim k^{\frac{1}{a}}, \tag{2.28}$$

a positive scaling with k, predicting that $x(k \to \infty) \to \infty$, namely that a node's activity increases with its degree. Consequently, under a sufficiently large $\kappa_{\rm nn}$, the nearest neighbor activity $x_{\rm nn}$ also diverges as $\kappa_{\rm nn}^{1/a}$, or alternatively, as $q_\odot^{-1/a}$. Hence we write

$$M_2(x_{\rm nn}) = \frac{x_{\rm nn}^h}{1+x_{\rm nn}^h} \sim \frac{q_\odot^{-\frac{h}{a}}}{1+q_\odot^{-\frac{h}{a}}} = \frac{1}{1+q_\odot^{\frac{h}{a}}} = 1 - q_\odot^{\frac{h}{a}} + \cdots , \tag{2.29}$$

observing directly that the leading power of $M_2(x_{\rm nn})$, and therefore also of $M_2(Z^{-1}(x))$ is $\Psi(0) = 0$. As a result, we obtain, using (1.66) our final exponent

$$\eta = -\Psi(0)(\mu - \nu - \rho) = 0. \tag{2.30}$$

This is, in fact, precisely the case of *Bounded* $M_2(x)$, discussed in Sec. 1.4.1, for which we *a priori* predicted $\eta = 0$.

2.3 Ecological dynamics

We consider mutualistic eco-systems, such as plant-pollinator networks, in which the interacting species exhibit symbiotic relationships. The species populations follow the dynamic equation

$$\frac{{\rm d}x_i}{{\rm d}t} = Bx_i(t)\left(1 - \frac{x_i(t)}{K}\right) + \sum_{j=1}^{N} A_{ij}x_i(t)F\big(x_j(t)\big). \tag{2.31}$$

The self dynamics

$$M_0(x) = Bx\left(1 - \frac{x}{K}\right) \tag{2.32}$$

captures logistic growth: when the population is small, the species reproduce at a rate B, yet, as x_i approaches the carrying capacity of the system K, growth is hindered by competition over limited resources [11]. The mutualistic inter-species interactions are captured by $M_1(x) = x$ and $M_2(x) = F(x)$, where $F(x)$ represents the *functional response*, describing the positive impact that species j has on species i. This functional response can take one of several forms [12]:

Type I: linear impact

$$F(x) = x. \tag{2.33}$$

Type II: saturating impact

$$F(x) = \frac{x}{1+x}. \tag{2.34}$$

Type III: a generalization of Type II, where

$$F(x) = \frac{x^h}{1+x^h}. \tag{2.35}$$

In our simulations we used Type II mutualistic interactions, therefore

$$M_2(x) = \frac{x}{1+x}. \tag{2.36}$$

For simplicity, we set the coefficients to $B = K = 1$.

For $R(x), Y(x)$ and $Z(x)$ we have

$$R(x) = -\frac{M_1(x)}{M_0(x)} = \frac{1}{x-1} \tag{2.37}$$

$$Y(x) = M_1(x)R'(x) = -\frac{x}{(x-1)^2} \tag{2.38}$$

$$Z(x) = R(x)M_2(x) = \frac{x}{x^2-1}. \tag{2.39}$$

Inverting $R(x)$ and $Z(x)$, we write

$$R^{-1}(x) = \frac{x+1}{x}, \tag{2.40}$$

$$Z^{-1}(x) = \frac{1}{2x}\left(1+\sqrt{1+4x^2}\right), \tag{2.41}$$

where in $Z^{-1}(x)$ we choose the positive solution, corresponding to the non-zero fixed-point of (2.31). Next, we construct the Hahn expansions of (1.65) as

$$M_2\big(Z^{-1}(x)\big) = \frac{Z^{-1}(x)}{1+Z^{-1}(x)} = \frac{1+\sqrt{1+4x^2}}{2x+1+\sqrt{1+4x^2}} = 1 - x + \cdots \tag{2.42}$$

$$Y\big(R^{-1}(x)\big) = -\frac{R^{-1}(x)}{\big(R^{-1}(x)-1\big)^2} = x + x^2 \tag{2.43}$$

$$M_1\big(R^{-1}(x)\big) = \frac{x+1}{x} = x^{-1} + 1 \tag{2.44}$$

$$M_2'\big(R^{-1}(x)\big) = \frac{1}{\big(R^{-1}(x)+1\big)^2} = \frac{x^2}{4x^2+4x+1} = x^2 - 4x^3 + \cdots, \tag{2.45}$$

whose leading powers are $\Psi(0) = 0, \Gamma(0) = 1, \Pi(0) = -1$ and $\Theta(0) = 2$. Consequently,

Social	$\frac{dx_i}{dt} = -fx_i + \sum_{j=1}^{N} A_{ij} g(1-x_i)x_j$	$\Omega = (0, 1, -1, 0)$	$S = -\beta$
Regulatory	$\frac{dx_i}{dt} = -Bx_i^a + \sum_{j=1}^{N} A_{ij} \frac{x_j^h}{1+x_j^h}$	$\Omega = \left(0, \frac{a-1}{a}, 0, -\frac{h+1}{a}\right)$	$S = -\frac{h}{a}\beta$
Ecological	$\frac{dx_i}{dt} = Bx_i\left(1-\frac{x_i}{K}\right) + \sum_{j=1}^{N} A_{ij} x_i \frac{x_j}{1-x_j}$	$\Omega = (0, 1, 1, -2)$	$S = -\beta$
Biochemical	$\frac{dx_i}{dt} = F - Wx_i - \widetilde{B} \sum_{j=1}^{N} A_{ij} x_i x_j$	$\Omega = (-1, 1, -1, 0)$	$S_{\text{Neg}} = -\beta$

Figure 1: **Dynamic models - summary**. Our four dynamic models and their associated exponents Ω. For each model we also show the stability classifier S. For Biochemical we use S_{Neg}, see Sec. 3.2

the dynamic exponents in (1.66) are

$$\mu = 2 - \Gamma(0) = 1 \tag{2.46}$$

$$\nu = -\Pi(0) = 1 \tag{2.47}$$

$$\rho = -\Theta(0) = -2 \tag{2.48}$$

$$\eta = -\Psi(0)(\mu - \nu - \rho) = 0, \tag{2.49}$$

once again, predicting $\eta = 0$, this time thanks both to the *Bounded activities* ($0 < x_i < K$) and to the *Saturating* nature of the interaction function $M_2(x)$ (Sec. 1.4.1).

2.4 Biochemical dynamics

As a Biochemical model we consider protein-protein interactions (PPI), which are driven by three processes: $\phi \to P_i$, describing the synthesis of the ith protein P_i at a rate F; $P_i \to \phi$, describing protein degradation at rate W; $P_i + P_j \rightleftharpoons P_iP_j$ describing the binding and unbinding of a pair of interacting proteins at rates B and U respectively. The hetero-dimer P_iP_j undergoes degradation $P_iP_j \to \phi$ at rate Q. The dynamical equations for this system are [10, 13]

$$\frac{\mathrm{d}x_i}{\mathrm{d}t} = F - Wx_i(t) + \sum_{j=1}^{N} Ux_{ij}(t) - B\sum_{j=1}^{N} A_{ij}x_i(t)x_j(t) \tag{2.50}$$

$$\frac{\mathrm{d}x_{ij}}{\mathrm{d}t} = BA_{ij}x_i(t)x_j(t) - (U+Q)x_{ij}(t), \tag{2.51}$$

where $x_i(t)$ is the concentration of P_i and $x_{ij}(t)$ is the concentration of the hetero-dimer P_iP_j. Under time-scale separation we assume that the hetero-dimer concentration is at steady-state, setting $\mathrm{d}x_{ij}/\,\mathrm{d}t = 0$ in (2.51). This provides us with

$$\frac{\mathrm{d}x_i}{\mathrm{d}t} = F - Wx_i(t) - \tilde{B}\sum_{j=1}^{N} A_{ij}x_i(t)x_j(t), \tag{2.52}$$

where the effective binding rate is $\tilde{B} = QB/(U+Q)$. Hence, in the effective equation (2.52) we have $M_0(x) = F - Wx$, $M_1(x) = -\tilde{B}x$ and $M_2(x) = x$, providing the dynamic functions (1.64)

$$R(x) = -\frac{M_1(x)}{M_0(x)} = \frac{\tilde{B}x}{F - Wx} \tag{2.53}$$

$$Y(x) = M_1(x)R'(x) = -\frac{F\tilde{B}^2x}{(F - Wx)^2} \tag{2.54}$$

$$Z(x) = R(x)M_2(x) = \frac{\tilde{B}x^2}{F - Wx}. \tag{2.55}$$

The inverse functions are, therefore

$$R^{-1}(x) = \frac{Fx}{\tilde{B} + Wx} \tag{2.56}$$

$$Z^{-1}(x) = \frac{W}{2\tilde{B}}x\left(-1 + \sqrt{1 + \frac{4\tilde{B}F}{W^2x}}\right), \tag{2.57}$$

where in $Z^{-1}(x)$ we choose the positive solution, corresponding to the positive fixed-point of (2.52). We can now compose the functions in (1.65), obtaining

$$M_2\big(Z^{-1}(x)\big) = Z^{-1}(x) = \sqrt{\frac{F}{\tilde{B}}}x^{\frac{1}{2}} + \frac{W^2}{8\tilde{B}^2F^{\frac{1}{2}}}x^{\frac{3}{2}} + \cdots \tag{2.58}$$

$$Y\big(R^{-1}(x)\big) = -\frac{F\tilde{B}^2R^{-1}(x)}{\big(F - WR^{-1}(x)\big)^2} = F\tilde{B}^2x + F\tilde{B}Wx^2 \tag{2.59}$$

$$M_1\big(R^{-1}(x)\big) = -\frac{\tilde{B}Fx}{\tilde{B} + Wx} = -Fx + \frac{FW}{\tilde{B}}x^2 + \cdots \tag{2.60}$$

$$M_2'\big(R^{-1}(x)\big) = 1, \tag{2.61}$$

allowing us to extract the leading powers as $\Psi(0) = 1/2, \Gamma(0) = 1, \Pi(0) = 1$ and $\Theta(0) = 0$. These powers provide the dynamic exponents via (1.66), providing, for Biochemical

$$\mu = 2 - \Gamma(0) = 1 \tag{2.62}$$

$$\nu = -\Pi(0) = -1 \tag{2.63}$$

$$\rho = -\Theta(0) = 0 \tag{2.64}$$

$$\eta = -\Psi(0)(\mu - \nu - \rho) = -1. \tag{2.65}$$

3 Principle eigenvalue of $J_{ij} \in \mathbb{E}(A_{ij}, \Omega)$

The stability of Eq. (1.1) can be characterized by the principal eigenvalue λ of J_{ij} in (1.67) - (1.68). As the entries depend on k_i and k_j, the value of λ is driven by the limit of large k - specifically, in a degree-heterogeneous network, it is determined by the nearest neighbor degree $\kappa_{\rm nn}$, which can potentially diverge with the system size N as

$$\kappa_{\rm nn} \sim N^{\beta}. \tag{3.1}$$

As opposed to the *dynamic* exponents Ω, the exponent β is a *topological* exponent, determined by the network's degree distribution $P(k)$. In a scale-free network, for example β is extracted from (1.63).

To approximate this hub-periphery structure, we use a *star* network, in which a single hub is linked to

$$k = \kappa_{\rm nn} \sim N^{\beta} \tag{3.2}$$

peripheral nodes. This captures the environment of a typical hub in, *e.g.*, a scale-free network. Indeed, the hubs in a scale-free network can be viewed as a collection of weakly coupled *stars*, that are only sparsely linked to each other [14]. Under these conditions we have the $(k+1) \times (k+1)$ network

$$A_{ij} = \begin{bmatrix} 0 & 1 & 1 & \dots & 1 \\ 1 & 0 & 0 & \dots & 0 \\ \vdots & & \ddots & & \vdots \\ 1 & 0 & 0 & \dots & 0 \end{bmatrix}, \tag{3.3}$$

which using (1.67) and (1.68), provides the corresponding Jacobian as

$$J_{ij} = -C\tilde{\kappa}_{\rm nn}^{\eta} \begin{bmatrix} k^{\mu} & 0 & \dots & 0 \\ 0 & 1 & \dots & 0 \\ \vdots & & \ddots & \vdots \\ 0 & 0 & \dots & 1 \end{bmatrix} + \begin{bmatrix} 0 & k^{\nu} & \dots & k^{\nu} \\ k^{\rho} & 0 & \dots & 0 \\ \vdots & & \ddots & \vdots \\ k^{\rho} & 0 & \dots & 0 \end{bmatrix}, \tag{3.4}$$

where $C > 0$. In (3.4) we used $\tilde{\kappa}_{\rm nn}$ to express the nearest neighbor degree in our star construction, which is potentially distinct from $\kappa_{\rm nn}$ of the originally approximated scale-free network. Lacking an *a priori* estimate for this parameter we express is as

$$\tilde{\kappa}_{\rm nn} \sim N^{\alpha}, \tag{3.5}$$

leaving us a degree of freedom to later tune α such that the prediction from our star construction best captures the observed results from a real scale-free network. Hence, β, characterizing the star-hub (k), is extracted from A_{ij} via (3.1) and α is a tunable parameter, which we select for the star-model to best fit the complete scale-free network results.

We emphasize that the star approximation in (3.3) by no means captures the complete behavior of a real scale-free network, as indeed it represents but a crude representation of an isolated hub environment. However, our goal here is to examine stability vs. instability - a feature that only depends on the *sign* of the principal eigenvalue, not on its specific value, and is, therefore, insensitive to the detailed structure of A_{ij}. As we show in Fig. 4 of the main text, the star approximation, while highly stylized, is, indeed, sufficient to capture this J_{ij} characteristic.

To obtain the principal eigenvalue we solve the linear equation

$$J\mathbf{v} = \lambda\mathbf{v}. \tag{3.6}$$

Using the symmetry of (3.4), we seek a solution of the form $\mathbf{v} = (a, b, b, \dots, b)^{\top}$, allowing us to reduce (3.6) into

$$-C\tilde{\kappa}_{\rm nn}^{\eta} k^{\mu} a + k k^{\nu} b = \lambda a \tag{3.7}$$

$$k^{\rho} a - C\tilde{\kappa}_{\rm nn}^{\eta} b = \lambda b. \tag{3.8}$$

Note that in $\mathbf{v}$ the specific values of a, b have no significance, only the ratio a/b, as we are only interested in the *direction* of the eigenvector, not its magnitude. We therefore arbitrarily set $a = 1$, allowing us to solve (3.7) - (3.8) and obtain

$$\lambda = \frac{1}{2}\left(-C\tilde{\kappa}_{\rm nn}^{\eta}(k^{\mu}+1) + \sqrt{C^2\tilde{\kappa}_{\rm nn}^{2\eta}(k^{\mu}+1)^2 - 4C^2\tilde{\kappa}_{\rm nn}^{2\eta}k^{\mu} + 4k^{1+\nu+\rho}}\right), \tag{3.9}$$

where, of the two solutions, we selected only the one in which the square-root is added (rather than subtracted), as we seek the *largest* eigenvalue. Seeking the limit

$$\lim_{N\to\infty}\left(\lambda\right), \tag{3.10}$$

we use (3.2) and (3.5) to rewrite (3.9) as

$$\begin{aligned}\lambda \;\sim\; & \frac{1}{2}\Big(-CN^{\alpha\eta}\big(N^{\beta\mu}+1\big) \\ & + \sqrt{C^2N^{2\alpha\eta}(N^{\beta\mu}+1)^2+4\left[-C^2N^{2\alpha\eta+\beta\mu}+N^{\beta(1+\nu+\rho)}\right]}\Big),\end{aligned} \tag{3.11}$$

in which we replace $\tilde{\kappa}_{\rm nn}$ and k by N^{α} and N^{β}, respectively. In (3.11) we ignore the pre-factors of the N-scaling, focusing only on the powers (α,β), hence substituting the equality sign $=$ with the asymptotic scaling operator $\sim$.

The case where $\mu>0$. First we analyze λ under $\mu>0$. Here, we write $N^{\beta\mu}\gg 1$, simplifying (3.11) in the limit $N\to\infty$ into

$$\lambda\sim\frac{1}{2}\left(-CN^{\alpha\eta+\beta\mu}+\sqrt{C^2N^{2(\alpha\eta+\beta\mu)}+4\left[-C^2N^{2\alpha\eta+\beta\mu}+N^{\beta(1+\nu+\rho)}\right]}\right). \tag{3.12}$$

Extracting the common terms out of the product we rewrite (3.12) as

$$\lambda\sim\frac{1}{2}CN^{\alpha\eta+\beta\mu}\left(-1+\sqrt{1+4\left(-N^{-\beta\mu}+\frac{1}{C^2}N^{\sigma}\right)}\right), \tag{3.13}$$

where

$$\sigma=\beta\left(1+\nu+\rho-2\mu-2\frac{\alpha}{\beta}\eta\right). \tag{3.14}$$

Note that $N^{-\beta\mu}\leq 1$ in (3.13), as $\mu>0$. Therefore, in case $\sigma\geq 0$, the N^{σ} term dominates the r.h.s. of the equation, providing, under $N\to\infty$,

$$\lambda\sim\frac{C}{\sqrt{C^2}}N^{\frac{1}{2}\sigma+\alpha\eta+\beta\mu}, \tag{3.15}$$

which, since $C>0$ is guaranteed to be positive, *i.e.* the system is *unstable*.

Next we consider the case $\sigma<0$. Under these conditions $N^{\sigma}\ll 1$, allowing us to expand the square-root in (3.13) to first order, providing

$$\lambda \sim \frac{1}{2} C N^{\alpha\eta+\beta\mu} \left(-1 + 1 + 2 \left(-N^{-\beta\mu} + \frac{1}{C^2} N^{\sigma} \right) \right) = -C N^{\alpha\eta} + \frac{1}{C} N^{\sigma+\alpha\eta+\beta\mu}. \quad (3.16)$$

We can rewrite this in the form of Eq. (9) of the main text, obtaining

$$\lambda \sim N^{Q} \left(1 - \frac{C}{N^{S}} \right), \quad (3.17)$$

where

$$Q = \sigma + \alpha\eta + \beta\mu \quad (3.18)$$

$$S = \sigma + \beta\mu. \quad (3.19)$$

As N^Q is guaranteed to be positive, the sign of λ depends on S: in case $S > 0$ the negative term in (3.17) satisfies $CN^{-S} \ll 1$, and hence we have $\lambda \sim N^Q > 0$, an unstable dynamics. If however $S < 0$, we have $-CN^{-S} \to -\infty$, predicting $\lambda < 0$, regardless of C, an asymptotically stable system. Consequently the system is stable as long as $S < 0$, which using (3.19), and taking σ from (3.14), predicts the stability condition

$$\beta \left(1 + \nu + \rho - \mu - 2\frac{\alpha}{\beta}\eta \right) < 0. \quad (3.20)$$

This condition reduces stability into a small set of *relevant* parameters: β, characterizing the network topology A_{ij}, and $\Omega = (\eta, \mu, \nu, \rho)$, associated with the dynamics $M_0(x), M_1(x), M_2(x)$. The non-universal parameter C becomes irrelevant in the limit of sufficiently large N. Finally, α can be selected to tune the star approximation optimally to the case of a real scale-free A_{ij}, as we do below. Note that condition (3.20) can also be expressed as $\sigma + \beta\mu < 0$. This implies that if $\sigma > \beta\mu$ the system is unstable. This instability condition already contains the previously obtained condition of $\sigma > 0$, that led to Eq. (3.15). Therefore, Eq. (3.20) is sufficient to characterize the system's stability.

Finally, the case $S = 0$ in (3.17) represents sensitive stability, in which λ's value is not asymptotically defined, and rather it depends on the coefficient C. In this class, stability in no longer a characteristic of the dynamic *model*, but rather of its specific rate constants, as encapsulated within C. A trivial example is when $\beta = 0$, *i.e.* a non fat-tailed $P(k)$, for example - Erdős-Rényi. Indeed, as we discuss in the main text, in such networks, stability can be tuned by the model parameters, lacking a defined asymptotic behavior.

The case where $\mu \leq 0$. Here, we have $N^{\beta\mu} \leq 1$, and hence Eq. (3.11) can be approximated by

$$\lambda \sim \frac{1}{2} \left(-C N^{\alpha\eta} + \sqrt{C^2 N^{2\alpha\eta} + 4\left[-C^2 N^{2\alpha\eta+\beta\mu} + N^{\beta(1+\nu+\rho)} \right]} \right), \quad (3.21)$$

leading to

$$\lambda \sim \frac{1}{2} C N^{\alpha\eta} \left(-1 + \sqrt{1 + 4\left(-N^{\beta\mu} + \frac{1}{C^2} N^{\omega} \right)} \right), \tag{3.22}$$

where

$$\omega = \beta \left(1 + \nu + \rho - 2\frac{\alpha}{\beta}\eta \right). \tag{3.23}$$

Once again, we have $N^{\beta\mu} \leq 1$, this time since $\mu < 0$. Therefore, as before, if $\omega > 0$, λ becomes dominated by the N^{ω} term, following

$$\lambda \sim \frac{C}{\sqrt{C^2}} N^{\frac{1}{2}\omega + \alpha\eta}, \tag{3.24}$$

which is always positive, *i.e. unstable*. If, however, $\omega < 0$, we use a linear approximation to write

$$\lambda \sim \frac{1}{2} C N^{\alpha\eta} \left(-1 + 1 + 2\left(-N^{\beta\mu} + \frac{1}{C^2} N^{\omega} \right) \right) = -C N^{\alpha\eta + \beta\mu} + \frac{1}{C} N^{\omega + \alpha\eta}, \tag{3.25}$$

once again - a competition between a positive vs. a negative term. Collecting the powers we, again, rewrite (3.25) in the form

$$\lambda \sim N^{Q} \left(1 - \frac{C}{N^{S}} \right), \tag{3.26}$$

where this time

$$Q = \omega + \alpha\eta \tag{3.27}$$

$$S = \omega - \beta\mu. \tag{3.28}$$

Stability is ensured if, for $N \to \infty$, the negative term dominates, namely if $S < 0$. Using (3.23) to express ω this provides

$$\beta \left(1 + \nu + \rho - \mu - 2\frac{\alpha}{\beta}\eta \right) < 0, \tag{3.29}$$

recovering precisely the condition in (3.20).

Tuning α. The parameter α represents a degree of freedom, rooted in the fact that the star approximation captures an inaccurate depiction of a real scale-free network. This approximation can be optimized if we select α such that the star best captures the

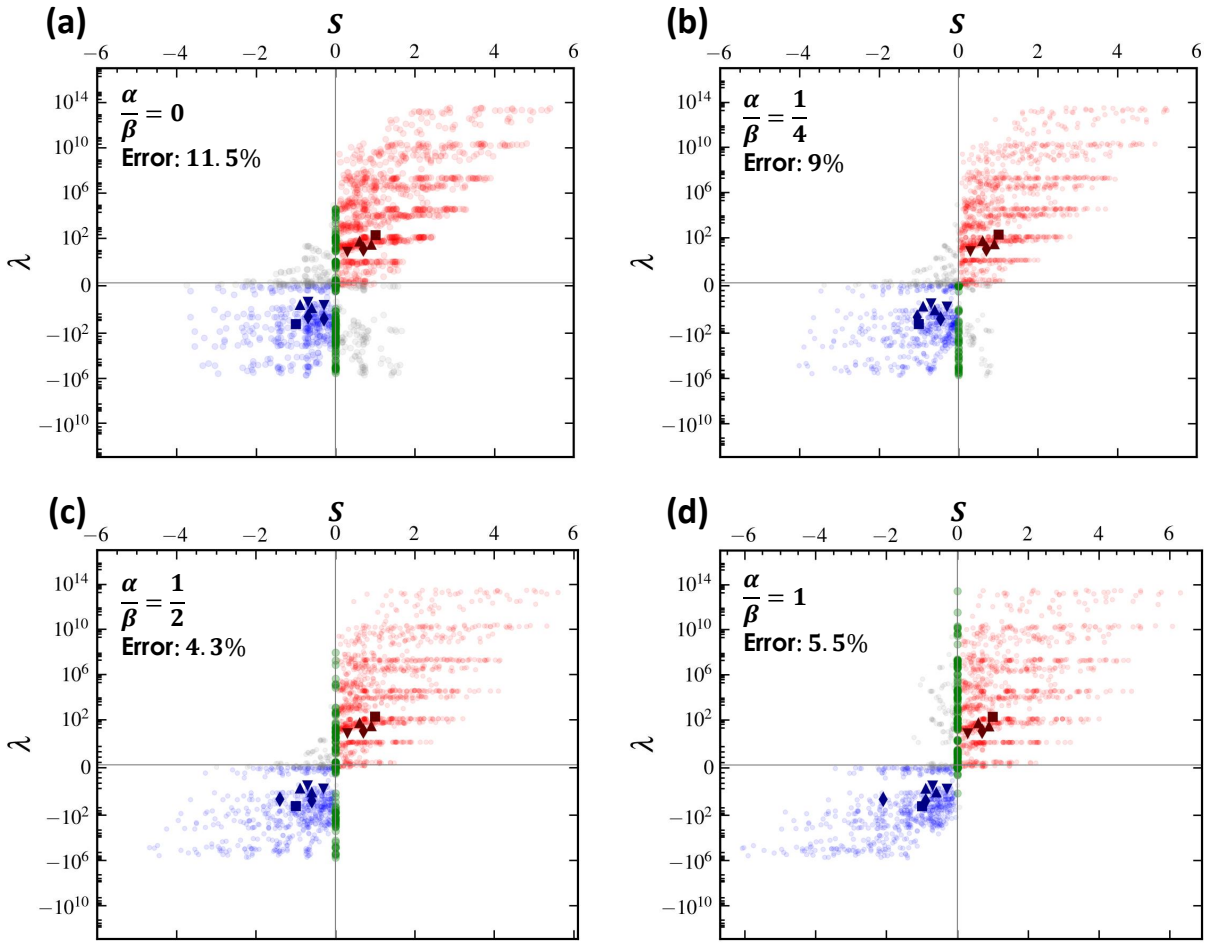

Figure 2: **Tuning the parameter** α. In Eqs. (3.20) and (3.29) we have the degree of freedom to set α/β for the star approximation to best predict the stability of complete scale-free networks. We used our set of $2,077$ J matrices (Fig. 4a of main text) to predict stability using different values of α/β. Quantifying the Error by the fraction of misclassified J matrices (grey dots), we find that setting $\alpha/\beta = 1/2$ provides the optimal fit, securing a $\sim 96\%$ correct classification (Error$= 4.3\%$).

complete scale-free network environment. We find that setting

$$\alpha = \frac{\beta}{2} \tag{3.30}$$

provides the optimal approximation, accurately predicting stability 96% of the time (Fig. 2). This completes the stability analysis, providing the stability classifier as

$$S = \beta\left(1 + \nu + \rho - \mu - \eta\right), \tag{3.31}$$

as appears in Eq. (10) of the main text.

3.1 The role of topology vs. dynamics

The stability condition (3.31) is driven by five distinct exponents. The first four exponents $\Omega = (\eta, \mu, \nu, \rho)$ are determined by the dynamic model - Social, Regulatory, Ecological etc. - intrinsic to the system's inherent interaction mechanisms. These exponents are independent of the topology A_{ij} or of microscopic model parameters, encapsulated within C, and are therefore *hardwired* into the system's dynamic behavior. For example, our formalism predicts that the SIS model (Social) has $\Omega = (0, 1, -1, 0)$ (Sec. 2.1). This prediction is characteristic of the SIS model, namely it is an intrinsic feature of the SIS interaction mechanisms of infection and recovery. It is, therefore, insensitive to the specific rates of the model - hence Ω remains unchanged if, *e.g.*, a disease has a high or low infection rate, or if it is transmitted via physical contact or aerosols. These will impact the constant C in (1.67), but will have no impact on the universal scaling. Similarly, Ω is unaffected by A_{ij}. Therefore, regardless of whether the disease spreads along the standard social network (Flu) or via sexual transmission (AIDS), as long as the *mechanism* is SIS (or any other mechanism for that matter) Ω remains the same.

The remaining exponent in (3.31), β, on the other hand, is independent of the dynamics, and determined solely by A_{ij}, specifically by its degree distribution $P(k)$, capturing the divergence of $\kappa_{\rm nn}$ in the limit of large N. For example, under a scale-free topology, where $P(k) \sim k^{-\gamma}$, we have $\kappa_{\rm nn}$ following Eq. (1.63), predicting

$$\beta = \begin{cases} 1 & \gamma < 2 \\ 3 - \gamma & 2 \leq \gamma < 3 \\ 0 & \gamma \geq 3 \end{cases} . \tag{3.32}$$

Therefore under $\gamma \geq 3$, we have $\beta = 0$ and stability becomes sensitive to parameters (C). On the other hand, under a scale-free topology ($\gamma < 3$) we observe the asymptotic stability/instability driven by $S \neq 0$.

3.2 Stability classifier S under negative interactions

Our formalism is designed to treat cooperative interactions, in which the interaction term $A_{ij}M_1(x_i)M_2(x_j) > 0$. Strictly speaking, our analysis is not designed to treat adversarial interactions, in which the mean-field derivation of Sec. 1 may fail to capture the complex patterns of all activities $x_i(t)$. Specifically, in the presence of negative interactions the steady-states x_i cannot always be expressed as a single variable function of k_i, as appears in Eq. (1.18). Rather, it also depends on i's neighborhood, *e.g.*, if the neighborhood has high activities, the adversarial interactions will drive x_i to be small, and vice versa. In certain cases, such as in our Biochemical model, this effect is marginal, all neighborhoods have (roughly) the same activity, and hence our analysis continues to apply. The star approximation, however, cannot distinguish between positive and negative interactions - as the derivation yields an identical outcome in both cases. Indeed, this approximation overlooks the potentially stabilizing effect of the negative off-diagonal terms.

Therefore, for simplicity, to evaluate S under negative interactions we consider a fully connected network of

$$k \sim N^{\beta} \tag{3.33}$$

nodes, *à la* May's original formulation. This simplification may not allow us to fully evaluate the contribution of A_{ij}, as, indeed, we have replaced the network by a single large clique, however, we are only interested in the stability of the *dynamics*, which remains independent of this simplifying assumption. With *all* nodes now having degree k, the resulting Jacobian takes the form

$$J_{ij} = -Ck^{\eta}\begin{bmatrix} k^{\mu} & 0 & \dots & 0 \\ 0 & k^{\mu} & \dots & 0 \\ \vdots & & \ddots & \vdots \\ 0 & 0 & \dots & k^{\mu} \end{bmatrix} - \begin{bmatrix} 0 & k^{\nu+\rho} & \dots & k^{\nu+\rho} \\ k^{\nu+\rho} & 0 & \dots & k^{\nu+\rho} \\ \vdots & & \ddots & \vdots \\ k^{\nu+\rho} & k^{\nu+\rho} & \dots & 0 \end{bmatrix}, \tag{3.34}$$

in which both the diagonal and the off-diagonal terms are preceded by a minus sign.

For a matrix of the form (3.34) the principal eigenvector is $\mathbf{v} = (1, -1, 0, \dots, 0)^{\top}$, whose associated eigenvalue is

$$\lambda = -Ck^{\eta+\mu} + k^{\nu+\rho}. \tag{3.35}$$

Using (3.33) we rewrite (3.35) in the form

$$\lambda = N^{Q_{\text{Neg}}}\left(1 - \frac{C}{N^{S_{\text{Neg}}}}\right), \tag{3.36}$$

where now

$$Q_{\text{Neg}} = \beta(\nu+\rho) \tag{3.37}$$

$$S_{\text{Neg}} = \beta(\nu+\rho-\mu-\eta). \tag{3.38}$$

Hence under negative dynamics the stability classifier is different from (3.29), being $S_{\text{Neg}} = S - \beta$. For example, in Biochemical, where $\Omega = (-1, 1, -1, 0)$ we have $S_{\text{Neg}} = -\beta < 0$, predicting a stable dynamics.

4 Methods and data analysis

4.1 Numerical integration

To numerically test our predictions we constructed Eq. (1.1) for each of the systems in Sec. 2, using the appropriate A_{ij} (Scale-free, Erdős-Rényi, empirical, etc.). We then used a fourth-order Runge-Kutta stepper (Matlab's ode45) to numerically solve the resulting equations. Starting from an arbitrary initial condition $x_i(t=0)$, $i = 1, \ldots, N$ we allowed the system to reach steady-state by waiting for $\dot{x}_i \to 0$. To numerically realize this limit we implemented the termination condition

$$\max_{i=1}^{N} \left| \frac{x_i(t_n) - x_i(t_{n-1})}{x_i(t_n)\Delta t_n} \right| < \varepsilon, \tag{4.1}$$

where t_n is the time stamp of the nth Runge-Kutta step and $\Delta t_n = t_n - t_{n-1}$. As the system approaches a steady-state, the activities $x_i(t_n)$ become almost independent of time, and the numerical derivative $\dot{x}_i = x_i(t_n) - x_i(t_{n-1})/\Delta t_n$ becomes small compared to $x_i(t_n)$. The condition (4.1) guarantees that the maximum of $\dot{x}_i/x_i$ over all activities $x_i(t_n)$ is smaller than the pre-defined termination variable ε. In our simulations, across the different dynamics we tested, we set $\varepsilon \leq 10^{-12}$, a rather strict condition, to ensure that our system is sufficiently close to the *true* steady-state.

4.2 Numerically estimating J_{ij}

Once the steady state $\mathbf{x} = (x_1, \ldots, x_N)^\top$ is reached we construct the *numerical* Jacobian by substituting the numerically obtained states x_i into (1.35) and (1.46). This represents the system's actual stability matrix, incorporating its specific dynamics on the relevant network A_{ij}. For example, consider our Social model in Eq. (2.3), where $M_0(x) = -fx, M_1(x) = 1 - x$ and $M_2(x) = gx$, and hence $M_0'(x) = -f, M_1' = -1$ and

$M_2' = g$. Once we obtain $\mathbf{x}$ we introduce all numerically calculated x_i into D_{ii} and W_{ij}, which for Social take the form

$$D_{ii} = -f + -\sum_{j=1}^{N} A_{ij} g x_j \tag{4.2}$$

and

$$W_{ij} = A_{ij}(1 - x_i)g. \tag{4.3}$$

In Fig. 2 of the main text we compare the scaling of these numerically estimated D_{ii} and W_{ij} vs. the theoretically predicted ensemble $\mathbb{E}(A_{ij}, \Omega)$, shown in (1.67) and (1.68).

4.3 Logarithmic binning

Our main theoretical prediction focuses on scaling relationships, such as $D(k) \sim k^{\mu}$, which we observe by their linear slope in a log-log plot. To construct such plots we employed logarithmic binning [15]. First we divide all nodes into B bins

$$\mathbb{B}(b) = \left\{ i = 1, \ldots, N \middle| c^{b-1} < k_i \leq c^b \right\}, \tag{4.4}$$

where $b = 1, ..., B$ and c is a constant. In (4.4) the bth bin includes all nodes i whose degrees k_i are between c^{b-1} and c^b. The parameter c is selected such that the unity of all bins $\cup_{b=1}^{B} \mathbb{B}(b)$ includes all nodes, hence we set $c^B = \max_{i=1}^{N} k_i$. We then plot the average degree of the nodes in each bin

$$k_b = \langle k_i \rangle_{i \in \mathbb{B}(b)} = \frac{1}{|\mathbb{B}(b)|} \sum_{i \in \mathbb{B}(b)} k_i \tag{4.5}$$

versus the average $D(k)$ term of nodes in that bin

$$D(k_b) = \langle D_{ii} \rangle_{i \in \mathbb{B}(b)} = \frac{1}{|\mathbb{B}(b)|} \sum_{i \in \mathbb{B}(b)} D_{ii}. \tag{4.6}$$

In a similar fashion we plot $W_{ij} \sim k_i^{\nu} k_j^{\rho}$, this time applying the binning on $k_i^{\nu} k_j^{\rho}$, instead of k_i. Therefore, the bins are defined as

$$\mathbb{B}(b) = \left\{ (i,j) \middle| A_{ij} = 1, c^{b-1} < k_i^{\nu} k_j^{\rho} \leq b^w \right\}, \tag{4.7}$$

such that in each bin we include all node pairs whose product $k_i^{\nu} k_j^{\rho}$ is within a given range. As above, we then plot the average W_{ij} in each bin, providing the real Jacobian terms

$$J_b^{\rm Real} = \langle W_{ij} \rangle_{(i,j)\in\mathbb{B}(b)} = \frac{1}{|\mathbb{B}(b)|} \sum_{(i,j)\in\mathbb{B}(b)} W_{ij} \tag{4.8}$$

vs. the average value of $k_i^\nu k_j^\rho$ in that bin

$$J_b^{\rm Th} = \langle k_i^\nu k_j^\rho \rangle_{(i,j)\in\mathbb{B}(b)} = \frac{1}{|\mathbb{B}(b)|} \sum_{(i,j)\in\mathbb{B}(b)} k_i^\nu k_j^\rho. \tag{4.9}$$

4.4 Model and empirical networks

To test our predictions we used model and real networks, as summarized below:

ER. An Erdős-Rényi random network with $N = 6,000$ nodes and an average degree of $\langle k \rangle = 6$.

SF1,2,3. A set of binary scale-free networks, constructed via the configuration model [2], with $N = 6,000$ nodes, $\langle k \rangle = 6$ and degree distribution following $P(k) \sim k^{-\gamma}$ with $\gamma = 2, 2.5$ and 3, respectively.

UCIonline (Social). An instant messaging network from the University of California Irvine [16], capturing $61,040$ transactions between $1,893$ users during a $T = 218$ day period. Connecting all individuals who exchanged messages throughout the period, we obtain a network of $1,893$ nodes with $27,670$ links, exhibiting a fat-tailed degree distribution.

Email Epoch (Social). This dataset monitors $\sim 3 \times 10^5$ emails exchanged between $3,185$ individuals over the course of ~ 6 months [17], giving rise to a scale-free social network with $31,885$ binary links.

PPI1 (Regulatory, Biochemical). The yeast scale-free protein-protein interaction network, consisting of $1,647$ nodes (proteins) and $5,036$ undirected links, representing chemical interactions between proteins [18].

PPI2 (Regulatory, Biochemical). The human protein-protein interaction network, a scale-free network, consisting of $N = 2,035$ nodes (protein) and $L = 13,806$ protein-protein interaction links [19].

ECO1,2 (Ecological). To construct the mutualistic ecological networks we collected data on symbiotic interactions of plants and pollinators in Carlinville Illinois from [20]. The resulting $456 \times 1,429$ network M_{ik} is a bipartite graph linking the 456 plants with their $1,429$ pollinators. When a pair of plants is visited by the same pollinator they mutually benefit each other indirectly, by increasing the pollinator populations. Similarly pollinators sharing the same plants also posses an indirect mutualistic interaction. Hence we can collapse M_{ik} to construct two mutualistic networks: The $1,429 \times 1,429$ pollinator network ECO1 and the 456×456 plant network ECO2. The resulting networks are

$$B_{kl} = \sum_{i=1}^{456} \frac{M_{ik} M_{il}}{\sum_{s=1}^{n} M_{is}}, \tag{4.10}$$

for the pollinator network (ECO1), and

$$A_{ij} = \sum_{k=1}^{1,429} \frac{M_{ik} M_{jk}}{\sum_{s=1}^{n} M_{sk}}, \tag{4.11}$$

for the plant network (ECO2). In both networks the numerator equals to the number of mutual plants (B_{kl}) or pollinators (A_{ij}). For each mutual plant i (pollinator k) we divide by the overall number of plants (pollinators) that share i (k). Hence, the weight of the mutualistic interaction in, *e.g.*, A_{ij} is determined by the density of mutual symbiotic relationships between all plants, where: (i) the more mutual pollinators k that plants i and j share the stronger the mutualistic interaction between them; (ii) on the other hand the more plants pollinated by k the smaller is its contribution to each plant. A similar logic applies also for the pollinator network B_{ij}. This process potentially allows us to have isolated components, *e.g.*, single disconnected nodes. The state of these isolated nodes is decoupled from the state of the rest of the network, and hence in our analysis we only focused on the giant connected component of A_{ij} and B_{ij}, comprising all 456 plants, rendering A_{ij} to be a fully connected component, but only $1,044$ pollinators, eliminating 385 isolated pollinators in B_{ij}.

5 Mixed dynamics

Our analytical derivation revolves around cooperative interactions, in which $A_{ij} \in \{0, 1\}$, *i.e.* non-negative, and the functions $M_1(x), M_2(x)$ in (1.1) are also positive for all x. The only exception is our Biochemical model, in which the hetero-dimer interaction $(-A_{ij} x_i x_j)$ captures depletion of i and j, and hence all interactions are negative. Some applications, however, involve a mixture of cooperative and adversarial interactions, requiring us to analyze signed networks in which $A_{ij} \in \{-1, 0, 1\}$. A classic example is in population dynamics, which, in many cases, represent a mixture of mutualistic interactions, coexisting alongside competitive and predatory dynamics. Strictly speaking, under these conditions, the Jacobian J_{ij} cannot be be extracted from the $\mathbb{E}(A_{ij}, \Omega)$ ensemble. Yet, as we next show, even then, our theory can still help us understand the emergence of stability.

Consider the Ecological model

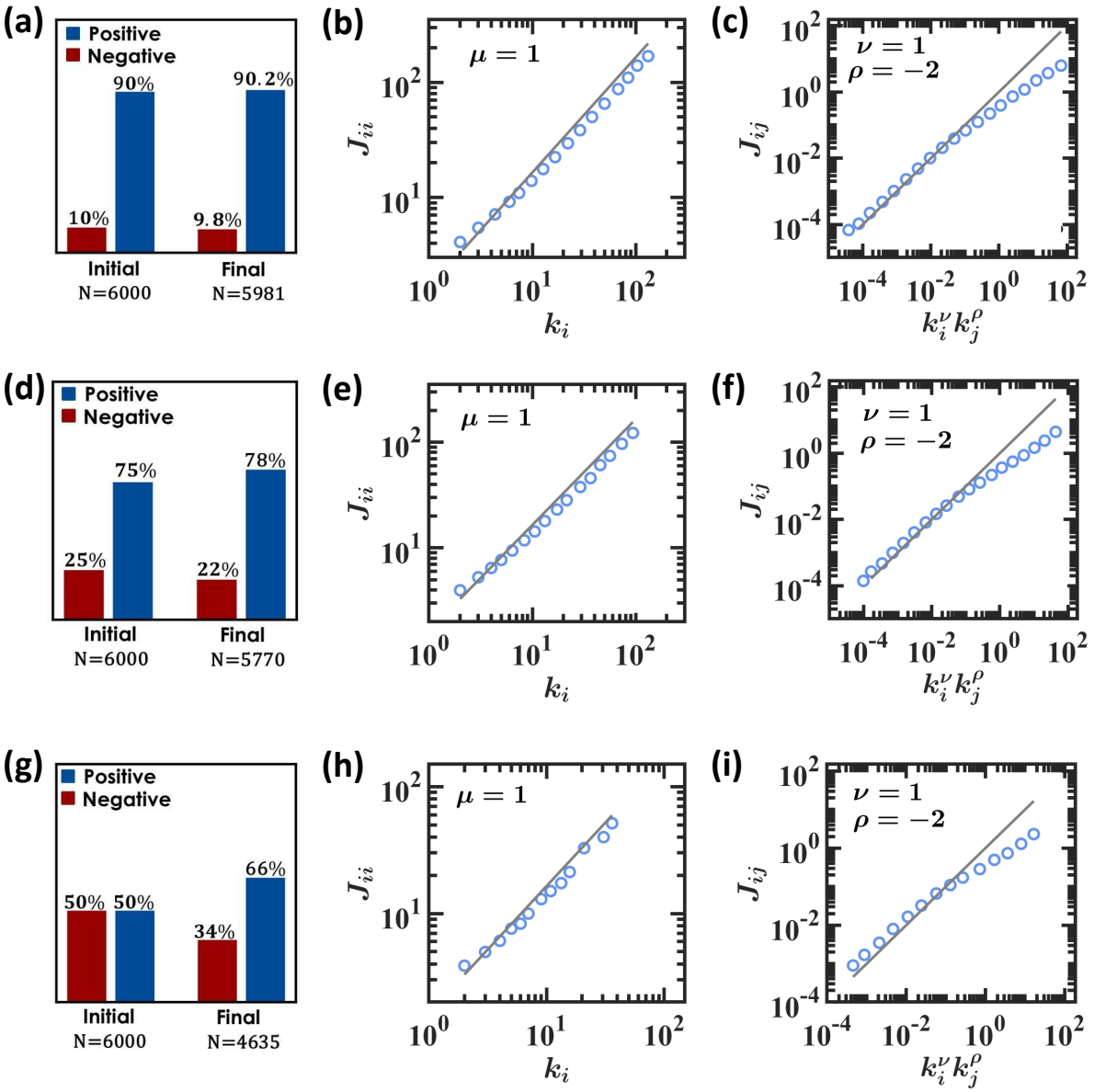

Figure 3: **Emerging stability under mixed interactions**. (a) Starting with a scale-free A_{ij} with 10% negative links, the system reaches a fixed-point in which nodes with many negative links become extinct. As a result the surviving $5,981$ node-network is slightly biased towards positive links (9.8% vs. the initial 10% negative). (b) The Jacobian matrix continues to follow the analytically predicted scaling $J_{ii} \sim k_i^\mu$, selectively for the (majority) of positive k_i. (c) Similarly the off-diagonal terms also follow the predicted $J_{ij} \sim k_i^\nu k_j^\rho$ (for $k_i, k_j > 0$) . (d)-(f) Similar analysis for an initial 25% negative links. (g)-(i) Even under 50% negative links the surviving network Jacobian ($4,635$ nodes) can still be approximated by $\mathbb{E}(A_{ij}, \Omega)$.

$$\frac{\mathrm{d}x_i}{\mathrm{d}t} = Bx_i(t)\left(1 - \frac{x_i(t)}{K}\right) + \sum_{j=1}^{N} A_{ij}x_i(t)\frac{x_j}{1+x_j}, \tag{5.1}$$

in which the the existing links in A_{ij} include a random fraction of $0 \leq f \leq 1$ negative interactions ($A_{ij} = -1$) and a remaining $1 - f$ fraction of links that are positive ($A_{ij} = 1$). As the system evolves in time, the activities $x_i(t)$ are positively impacted by the cooperative interactions, but suppressed by the adversarial ones. Therefore, nodes with many negatively interacting partners will have their activities driven towards $x_i(t) \to 0$. The crucial point is that once a node reaches zero activity, it becomes extinct, and effectively removed from the network, together with its set of links. As a consequence the system will reach a steady state, in which the surviving nodes are biased towards positive k_i. *This represents a quite general, and most importantly, a naturally emerging organizing principle that leads real world A_{ij} to have a majority positive set of links.*

To exemplify this, we constructed a scale free A_{ij} with $N = 6,000$ nodes and $L = 18,000$ links, of which a fraction $f = 0.1$ are negative, representing a 10% adversarial network. Starting from an arbitrary initial condition, we allowed the system (5.1) to naturally reach its fixed-point. During the process, whenever a specific activity reached $x_i(t) \leq \epsilon$ we set it permanently to zero (extinction), effectively removing it from the network; we used $\epsilon = 10^{-12}$. At its final state the network is reduced to $N = 5,981$ surviving nodes, featuring a (slight) decrease in the fraction of negative links, from 10% to 9.8% (Fig. 3a). This is a minor effect, of course, however, as we increase the negative link fraction, f, this positive-link bias becomes more pronounces. Indeed, under an initial condition where $f = 0.25$, the system reached a final state in which the negative links are reduced to 22% (Fig. 3d), and, finally, starting with a balanced positive-negative network ($f = 0.5$), we find, after pruning the extinct nodes, that the final surviving network is 66% positive (Fig. 3g).

For each of these three network, once reaching a fixed point, we extracted numerically their Jacobain matrix, as explained in Sec. 4.2. As expected, the resulting J matrices include both positive and negative weights, and hence, strictly speaking $J \notin \mathbb{E}(A_{ij}, \Omega)$. However, thanks to the pruning effect, the actual J matrices remain predominantly positive, and the majority of surviving nodes continue to have $k_i > 0$. Hence, while imperfect, we still observe that J follows (approximately) the scaling patterns of the $\mathbb{E}(A_{ij}, \Omega)$ ensemble. Indeed, Fig. 3b,c,e,f,h,i confirms that, despite the inclusion of negative links, J_{ii} and J_{ij} continue to follow (1.67) and (1.68) with $\mu = 1, \nu = 1$ and $\rho = -2$, as predicted for Ecological.

Taken together, this exemplifies that both under fully positive and under mixed interactions, real-world Jacobian matrices are, indeed, non-random, exhibiting (exactly or approximately) the unique interplay between topology and dynamics expressed in $\mathbb{E}(A_{ij}, \Omega)$. These patterns require no *devious strategies*, but rather arise from naturally emerging organizing principles: for positive dynamics - the scaling Ω, and for mixed interactions that,

in combination with the pruning of negative links via extinction.

References

[1] B. Barzel and A.-L. Barabási. Universality in network dynamics. *Nature Physics*, 9: 673 – 681, 2013.

[2] M.E.J. Newman. *Networks - an introduction*. Oxford University Press, New York, 2010.

[3] J. Gao, B. Barzel and A.-L. Barabási. Universal resilience patterns in complex networks. *Nature*, 530:307—-312, 2016.

[4] G. Caldarelli. *Scale-free networks: complex webs in nature and technology*. Oxfrod University Press, New York, 2007.

[5] S. Boccaletti, V. Latora, Y. Moreno, M. Chavez and D.-U. Hwang. Complex networks: Structure and dynamics. *Physics Reports*, 424:175–308, 2006.

[6] L. Schmetterer and K. Sigmund (Eds.). *Hans Hahn Gesammelte Abhandlungen Band 1/Hans Hahn Collected Works Volume 1*. Springer, Vienna, Austria, 1995.

[7] R.M. May. Will a large complex system be stable? *Nature*, 238:413 – 414, 1972.

[8] P.S. Dodds and D.J. Watts. A generalized model of social and biological contagion. *Journal of Theoretical Biology*, 232:587–604, 2005.

[9] G. Karlebach and R. Shamir. Modelling and analysis of gene regulatory networks. *Nature Reviews*, 9:770–780, 2008.

[10] B. Barzel and O. Biham. Binomial moment equations for stochastic reaction systems. *Phys. Rev. Lett.*, 106:150602–5, 2011.

[11] R.M. May. Simple mathematical models with very complicated dynamics. *Nature*, 261:459–467, 1976.

[12] C.S. Holling. Some characteristics of simple types of predation and parasitism. *The Canadian Entomologist*, 91:385–398, 1959.

[13] E.O. Voit. *Computational Analysis of Biochemical Systems*. Cambridge University Press, New York, NY, 2000.

[14] H.I. Schreier, Y. Soen and N. Brenner. Exploratory adaptation in large random networks. *Nature Communications*, 8:14826, 2017.

[15] S. Milojević. Power-law distributions in information science: making the case for logarithmic binning. *Journal of the American Society for Information Science and Technology*, 61:2417–2425, 2010.

[16] T. Opsahl and P. Panzarasa. Clustering in weighted networks. *Social Networks*, 31: 155–163, 2009.

[17] J.-P. Eckmann, E. Moses and D. Sergi. Entropy of dialogues creates coherent structures in e-mail traffic. *Proc. Natl. Acad. Sci. USA*, 101:14333–7, 2004.

[18] H. Yu *et al.* High-quality binary protein interaction map of the yeast interactome network. *Science*, 322:104–110, 2008.

[19] J.F. Rual *et al.* Towards a proteome-scale map of the human protein-–protein interaction network. *Nature*, 437:1173–1178, 2005.

[20] Interaction web database. http://www.nceas.ucsb.edu/interactionweb/resources.